

Hedgehog: An Isolated Quiescent Dwarf Galaxy at 2.4 Mpc

JIAOXUAN LI (李嘉轩) ¹, JENNY E. GREENE ¹, SCOTT G. CARLSTEN ¹, AND SHANY DANIELI ¹

¹*Department of Astrophysical Sciences, 4 Ivy Lane, Princeton University, Princeton, NJ 08544, USA*

ABSTRACT

It is well known that almost all isolated dwarf galaxies are actively forming stars. We report the discovery of Hedgehog, an isolated quiescent dwarf galaxy at a distance of 2.41 ± 0.14 Mpc with a stellar mass of $M_\star \approx 10^{5.8} M_\odot$. The distance is measured using surface brightness fluctuations with both Legacy Surveys and deep Magellan/IMACS imaging data. Hedgehog is 1.7 Mpc from the nearest galaxy group, Centaurus A, and has no neighboring galaxies within 1 Mpc, making it one of the most isolated quiescent dwarfs at this stellar mass. It has a red optical color, early-type morphology, and shows no UV emission. This indicates that Hedgehog has an old stellar population and is quiescent in star formation. Compared with other quiescent dwarfs in the Local Group and Local Volume, Hedgehog appears smaller in size for its luminosity but is consistent with the mass–size relations. Hedgehog might be a backsplash galaxy from the Centaurus A group, but it could also have been quenched in the field by ram pressure stripping in the cosmic web, reionization, or internal processes such as supernova and stellar feedback. Future observations are needed to fully unveil its formation, history, and quenching mechanisms.

Keywords: Dwarf galaxies (796); Galaxy quenching (2040); Galaxy evolution (594); Galaxy distances (590).

1. INTRODUCTION

Low-mass dwarf galaxies are fragile objects. Their star formation can be halted by internal processes (e.g., stellar feedback; Hopkins et al. 2012; El-Badry et al. 2018), and external processes (e.g., tidal and ram-pressure stripping; Gunn & Gott 1972; Simpson et al. 2018), and reionization (Bullock et al. 2000; Ricotti & Gnedin 2005; Applebaum et al. 2021). Consequently, dwarf galaxies serve as sensitive probes for understanding both baryonic physics and environmental effects.

All satellite dwarf galaxies of the Milky Way, except for the Large and Small Magellanic Clouds, are quiescent (e.g., McConnachie 2012; Karachentsev et al. 2013; Wetzel et al. 2015). In contrast, quiescent dwarfs are found to be exceptionally rare ($< 0.06\%$) among the isolated dwarfs with $M_\star = 10^{7-9} M_\odot$ (Geha et al. 2012). Despite their rarity, several isolated quiescent dwarf galaxies have been discovered. Some are located on the outskirts of the Local Group (e.g., Cetus, Tucana, And XVIII, Eri II; McConnachie 2012) and M81

(e.g., Blobby; Casey et al. 2023). Others are found far from any massive galaxy (e.g., KKR 25, Makarov et al. 2012; KKs 3, Karachentsev et al. 2015; COSMOS-dw1, Polzin et al. 2021; UGC 5205, Kado-Fong et al. 2024; PEARLSDG, Carleton et al. 2024). While the majority of these dwarfs are confirmed to be in the field by measuring distances using the tip of the red-giant branch (TRGB), the surface brightness fluctuation (SBF; Tonry & Schneider 1988; Carlsten et al. 2019; Greco et al. 2021) technique has recently become an efficient new method for discovering these galaxies, including COSMOS-dw1 (Polzin et al. 2021) and Blobby (Casey et al. 2023).

The mechanisms by which these isolated dwarfs are quenched remain unclear. One possible explanation is that these dwarfs might have already entered the virial radius of a bigger group, experienced one pericenter passage, and then were ejected into the field. Consequently, they could be quenched due to close interactions with the host halo (Teyssier et al. 2012). Simulations suggest that these so-called “backsplash” dwarf galaxies can be found out to ~ 2.5 times the virial radius (Wetzel et al. 2014; More et al. 2015; Buck et al. 2019; Applebaum et al. 2021; Benavides et al. 2021). On the other hand, isolated dwarf galaxies could be quenched via

ram pressure when they move through the cosmic web (Benítez-Llambay et al. 2013). Stellar feedback might also temporarily halt star formation (El-Badry et al. 2018). Ultra-faint dwarfs in the field can be quenched by reionization alone (e.g., Tucana B; Sand et al. 2022).

In this Letter, we report the discovery of Hedgehog, an isolated quiescent dwarf galaxy at a distance of $D \approx 2.4$ Mpc. With no neighboring galaxies within 1 Mpc and located 1.7 Mpc from the nearest massive galaxy group (4–5 times the virial radius of the group), Hedgehog is one of the most isolated quiescent dwarfs found to date. We present the discovery of this galaxy and our follow-up observations in Section 2. In Section 3, we measure the SBF distance to this dwarf galaxy using data from the DESI Legacy Imaging Surveys Data Release 10 (hereafter Legacy Surveys or LS DR10; Dey et al. 2019) and the deep high-resolution Magellan/IMACS imaging data. We show the 3-D environment of Hedgehog in Section 4, then present the physical properties and characterize the stellar population of Hedgehog in Section 5. We discuss possible quenching mechanisms in Section 6.

We adopt a flat Λ CDM cosmology with $\Omega_m = 0.3$ and $H_0 = 70 \text{ km s}^{-1} \text{ Mpc}^{-1}$. The virial radius (R_{vir}) of a dark matter halo is defined as the radius within which the average density is $\Delta = 200$ times the critical density. All photometry presented in this work is in the AB system (Oke & Gunn 1983). We apply corrections for the Milky Way dust extinction using the dust map in Schlegel et al. (1998) re-calibrated by Schlafly & Finkbeiner (2011). The solar absolute magnitudes used in this work are taken from Willmer (2018).

2. DISCOVERY, OBSERVATIONS, AND PHOTOMETRY

Hedgehog (dw1322m2053, following standard naming practice) was discovered serendipitously in the Legacy Surveys DR10 data when we searched for potential dwarf galaxies associated with NGC 5068 at $D = 5.15$ Mpc (Karachentsev et al. 2018). Located ~ 1 deg away from NGC 5068, Hedgehog was initially considered a satellite candidate of NGC 5068. As shown in the left panel of Figure 1, Hedgehog exhibits significant surface brightness fluctuation in Legacy Surveys DR10 data, strongly suggesting that it might be a foreground dwarf galaxy. It also has a red color and an early-type morphology without any star-forming regions, making it a possible candidate for an isolated quenched dwarf galaxy.

2.1. Follow-up observations

To determine the distance and the properties of Hedgehog, we conducted follow-up observations with

the Inamori Magellan Areal Camera and Spectrograph (IMACS; Dressler et al. 2011) on the 6.5-m Magellan Baade Telescope on April 01, 2024. Using the $f/2$ camera, which offers a field-of-view of $27.5'$ in diameter and a pixel scale of $0.2''$ per pixel, we obtained deep imaging data for Hedgehog in the Sloan i -band filter. We took four exposures of 5 minutes each and dithered between exposures to bridge the chip gaps. The seeing was about $0.5 - 0.6''$ during the observation. We reduced the data using a custom pipeline similar to that used in Carlsten et al. (2022). It includes bias subtraction and flat fielding correction using the twilight flat frames. The astrometric solution was obtained using ASTROMETRY.NET (Lang et al. 2010), and the local sky background was subtracted using SExtractor (Bertin & Arnouts 1996) with a mesh size of $51.2''$. We calibrated our photometry against the DECam Local Volume Exploration Survey (DELVE; Drlica-Wagner et al. 2021) DR2 photometric catalog (Drlica-Wagner et al. 2022), such that all photometry in this work is in the DECam filter system. In the end, we fine-tuned the astrometric solution using SCAMP (Bertin 2006) and co-added all exposures using SWARP (Bertin et al. 2002). A spatially-varying PSF model was constructed using PSFEX (Bertin 2011) and evaluated at the location of Hedgehog. The final co-added i -band image has a point-spread function (PSF) FWHM of $0.6''$, indicating that the PSF is marginally undersampled.

We show the co-added IMACS image in the middle panel of Figure 1. Hedgehog is resolved into individual stars thanks to the excellent seeing and depth. Unfortunately, we do not have follow-up data in bluer bands to construct a color-magnitude diagram (CMD) and determine the TRGB distance.

SBF measurements are sensitive to the noise properties of the image. As demonstrated in Mei et al. (2005), different interpolation kernels used during resampling in the co-addition process would significantly change the noise power spectrum and consequently affect the distance measurement. A commonly-used Lanczos3 kernel introduces noise correlation, causing the noise power spectrum to drop at a spatial frequency of $k \gtrsim 0.35 \text{ pix}^{-1}$ (Cantiello et al. 2005; Carlsten et al. 2019). This makes fitting for the noise level challenging, especially when the PSF is sharp and undersampled. To mitigate this issue, we use the nearest-neighbor interpolation kernel, which preserves the noise property of the original images. Since Hedgehog is well-covered by all the exposures, we do not find any aliasing or empty pixels in the co-added image around Hedgehog.

2.2. Optical Photometry and Structural Properties

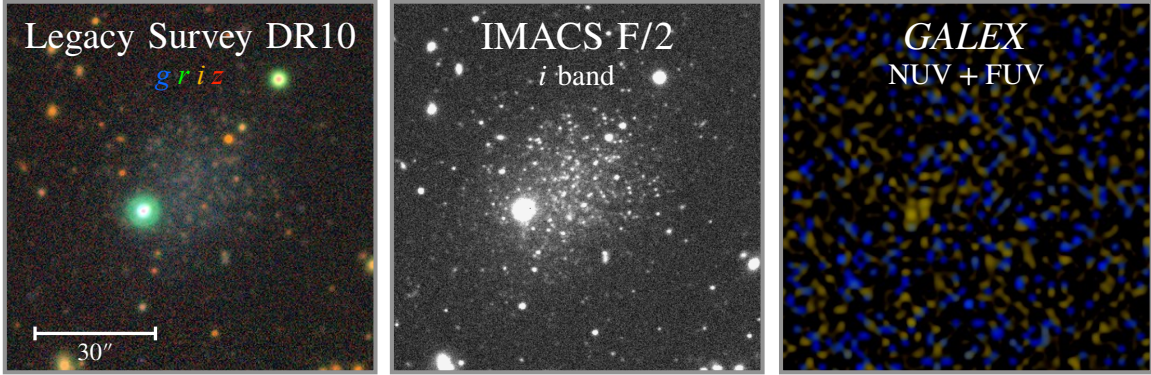


Figure 1. Cutout images of Hedgehog from the Legacy Surveys DR10 (left), the deep and high-resolution Magellan/IMACS i -band data (middle), and the Galaxy Evolution Explorer (*GALEX*) near-UV and far-UV data (right). Hedgehog shows significant surface brightness fluctuation signals in the Legacy Surveys data and is resolved into individual stars in the IMACS data. There is also no significant UV emission associated with Hedgehog.

Table 1. Properties of Hedgehog.

Parameter	Value
α_0 (J2000)	13:22:46.88
δ_0 (J2000)	-20:53:55.94
m_g (mag)	17.35 ± 0.06
$g - r$ (mag)	0.49 ± 0.04
$g - i$ (mag)	0.62 ± 0.04
r_{eff} (arcsec)	15.1 ± 0.8
$n_{\text{Sérsic}}$	0.56 ± 0.03
$\mu_{0,g}$ (mag arcsec $^{-2}$)	24.80 ± 0.15
Ellipticity	0.22 ± 0.03
SNR_{NUV}	1.8
m_{NUV} (mag)	> 17.5
SNR_{FUV}	0.7
m_{FUV} (mag)	> 19.00
Distance (Mpc)	2.41 ± 0.14
M_g (mag)	-9.56 ± 0.14
M_V (mag)	-9.84 ± 0.16
$\log(M_*/M_\odot)$	5.8 ± 0.2
r_{eff} (pc)	176 ± 14
$\log(\text{SFR}_{\text{NUV}}/M_\odot \text{ yr}^{-1})$	< -3.7
$\log(\text{SFR}_{\text{FUV}}/M_\odot \text{ yr}^{-1})$	< -4.5
$\log(M_{\text{HI}}/M_\odot)$	< 6.0

We measure the structural properties of Hedgehog by fitting a single Sérsic model to the Legacy Surveys DR10 data in the gri bands. This part of the Legacy Surveys data is primarily from the DELVE survey (Drlica-Wagner et al. 2021, 2022). It is much shallower and has

much worse seeing compared with our IMACS data¹. Similar to Carlsten et al. (2021), we directly take the co-added images and the corresponding PSF models from the Legacy Surveys DR10 for Sérsic fits using IMFIT (Erwin 2015).

We start with fitting a Sérsic model to the g -band image because it is deeper and has the least SBF signals (Carlsten et al. 2019; Greco et al. 2021). The free parameters include the central right ascension (α_0) and declination (δ_0), total g -band magnitude (m_g), effective radius (r_{eff} , measured along the semi-major axis), Sérsic index ($n_{\text{Sérsic}}$), and ellipticity (defined as $1 - b/a$). Subsequently, we fit the r - and i -band images using the best-fit Sérsic model from the g -band, fixing the structural parameters and allowing only the total magnitude to vary. To estimate potential measurement uncertainties and biases in photometry and structural parameters, we inject mock Sérsic galaxies into Legacy Surveys DR10 images and fit them using the same procedure described above (see Appendix A for details). We correct for measurement biases and list the photometry and structural parameters in Table 1.

2.3. *GALEX*

We search for possible UV emission from Hedgehog using data from the Galaxy Evolution Explorer (*GALEX*; Martin et al. 2005) survey, following the method described in Greco et al. (2018); Karunakaran et al. (2021); Carlsten et al. (2022). We first query the available images that overlap with Hedgehog on the Mikulski Archive for Space Telescopes (MAST) *GALEX* tile re-

¹ The seeing values are $1.3''$, $2.3''$, $1.3''$ in the gri bands, and the 5-sigma PSF detection depths are 24.9, 24.3, and 23.9 mags, respectively.

trieval service². Tile AIS.234_sg74, which has the longest exposure time ($t_{\text{NUV}} = 207.05\text{s}$, $t_{\text{FUV}} = 202.05\text{s}$) among the available tiles, is chosen for photometry. We download the intensity image (I) and the high-resolution relative response maps (R) from MAST and calculate the variance image $V = I/R$.

Using PHOTUTILS (Bradley et al. 2016), we perform circular aperture photometry for Hedgehog with a radius twice the effective radius from the Sérsic fits in §2.2. This aperture size includes most of the flux from the galaxy but not too much background noise. Since the intensity image is not background subtracted, we estimate the background value and its standard deviation. After masking out all bright sources using `sep` (Barbary 2016), we randomly place 100 apertures within 6 arcmin from the target galaxy. We calculate the median of the values in these apertures and subtract it from the intensity image. The standard deviation, σ_{sky} , represents the uncertainty from the sky background. We then do aperture photometry at the location of Hedgehog to measure the flux $F = \sum_i I_i$, where i ranges over all pixels in the aperture. The bright star near Hedgehog is masked. The uncertainty of the flux is then $\sigma_F = (\sum_i V_i + \sigma_{\text{sky}}^2)^{1/2}$, and the signal-to-noise ratio (SNR) is defined as $\text{SNR} = F/\sigma_F$. We convert the measured flux to AB magnitude taking the zero-points from Morrissey et al. (2007), and correct for Galactic extinction using $R_{\text{NUV}} = 8.2$ and $R_{\text{FUV}} = 8.24$ (Wyder et al. 2007).

The *GALEX* photometry results are listed in Table 1. We do not find significant emission in either NUV or FUV, with $\text{SNR} < 2$ for both bands. Therefore, we report the 2-sigma lower limits of the magnitudes in Table 1. We note that the *GALEX* data used here is relatively shallower than the data used in Karunakaran et al. (2022) and Carlsten et al. (2022).

3. DISTANCE

For Hedgehog, the most crucial information needed to determine the physical properties and environment is its distance. In this section, we measure the SBF distance to Hedgehog *independently* using both IMACS and Legacy Surveys DR10 i -band data. Here we briefly summarize the SBF measurement and refer interested readers to Carlsten et al. (2019), Carlsten et al. (2021), Greco et al. (2021), and references therein for more detailed descriptions of the SBF technique in the dwarf galaxy regime.

SBF measures the pixel-to-pixel variation in the image due to the Poisson fluctuations in the number of bright stars per resolution element. As distance increases, the number of stars per pixel grows, and the variance decreases. Thus, the SBF signal depends on distance and the stellar population of the galaxy. In addition, the fluctuation from the background galaxies and other unresolved sources contribute to the measured fluctuation and need to be masked.

In this work, we measure the SBF distance in the i -band since the SBF signal is stronger and the seeing is typically better. In practice, we first fit a smooth Sérsic model to the target galaxy (similar to §2.2), subtract it from the image, and normalize the residual image by dividing by the square root of the Sérsic model. To mask out globular clusters, background galaxies, and foreground stars, we use a certain absolute magnitude threshold M_i (Carlsten et al. 2019). Sources that are brighter than this threshold are masked. In this work, we set $M_i^{\text{IMACS}} = -4.0$ mag for IMACS data and $M_i^{\text{LS}} = -4.2$ mag for Legacy Surveys data assuming a distance of 2.4 Mpc. This ensures that globular clusters ($M_i \sim -8$ mag) are masked while the brightest red giant branch stars ($M_i \sim -4$ mag) are kept from masking.

Because the distance of Hedgehog is unknown, we adjust the assumed distance and the absolute magnitude threshold iteratively until it converges. The absolute magnitude thresholds are different for IMACS and Legacy Surveys because of their different resolution and depth. Using a fainter threshold for the Legacy Surveys data will mask too many regions contributing to the SBF signal. To maximize the signal-to-noise ratio, we also mask out regions where the surface brightness of the galaxy falls below 0.25 times the central surface brightness. The yellow color in the left panels of Figure 2 highlights the mask. The IMACS and Legacy Surveys masks agree with each other quite well. The masked sources include a bright foreground star and likely several Galactic M-dwarf stars because of their very red colors (Figure 1). The middle panel shows the masked normalized residual maps.

We compute the azimuthally averaged power spectrum of the masked normalized residual image, shown as the blue solid line in the right panel of Figure 2. We then fit it with a combination of the power spectrum of the PSF and a constant white noise floor (red dashed lines in Figure 2). The desired SBF signal is the coefficient of the PSF component. For dwarf galaxies with low surface brightness, the unmasked contaminating sources would significantly contribute to the measured SBF signal. We further estimate the contribution from the residual contaminating sources by measuring the SBF signals from

² <https://galex.stsci.edu/GR6/?page=tilelist&survey=ais&showall=Y>

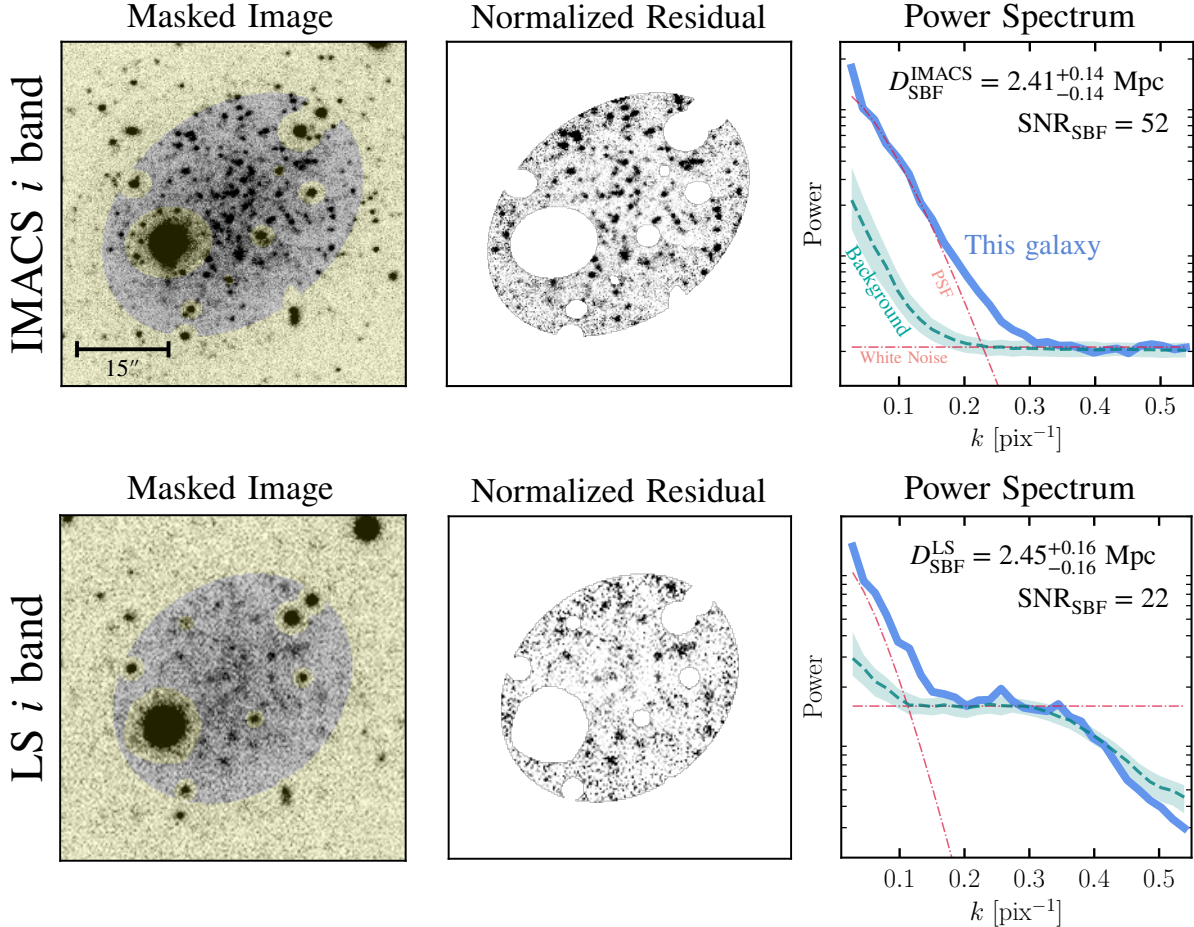


Figure 2. The surface brightness fluctuation (SBF) measurements for Hedgehog using the IMACS *i*-band data (top panel) and the Legacy Surveys DR10 *i*-band data (bottom panel). The left panel shows the original image with the mask overlaid in yellow. We fit a Sérsic model to the masked image, subtract the model from the image, and divide the residual by the square root of the model. This normalized residual image is shown in the middle panel. We then calculate the azimuthally averaged power spectrum of the normalized residual, as shown in the right panel. The power spectrum is fit with a combination of the PSF power spectrum and white noise. To account for the contribution from unmasked sources, we measure SBF signals on randomly selected blank fields, whose power spectra are shown as the teal dashed line. After subtracting the background, we calculate the median SBF signal and its standard deviation. The SBF distances from IMACS and Legacy Surveys DR10 are $D_{\text{SBF}}^{\text{IMACS}} = 2.41 \pm 0.14$ Mpc, $D_{\text{SBF}}^{\text{LS}} = 2.45 \pm 0.16$ Mpc. These two independently-measured distances are fully consistent.

randomly selected blank fields around the target galaxy. For blank fields, we construct the normalized residual image using the Sérsic model from the target galaxy and use the same masking threshold to generate masks. The signals from the blank fields are subtracted from the measured SBF signal. The teal-shaded region in Figure 2 demonstrates the power spectrum of the background fields.

To characterize the uncertainty of the SBF measurement, we adopt a Monte Carlo approach by randomly sampling the location of the background fields and the spatial frequency range used for the power spectrum fit-

ting (Cohen et al. 2018)³. The lower spatial frequency follows $k_1 \sim \mathcal{U}(0.03, 0.08)$ pix^{-1} . The upper spatial frequency follows $k_2 \sim \mathcal{U}(0.35, 0.45)$ pix^{-1} for IMACS, but follows $k_2 \sim \mathcal{U}(0.3, 0.4)$ pix^{-1} for Legacy Surveys because the correlated noise in the Legacy Surveys image becomes prominent around $k \gtrsim 0.35$ pix^{-1} . We did 100 Monte Carlo runs, and took the median value of the background-corrected SBF signals to be the measured SBF signal, and their standard deviation to be the un-

³ For IMACS, we also tried sampling the absolute magnitude threshold for generating the mask $M_i \sim \mathcal{U}(-3.9, -4.1)$. It lowers the SBF signal-to-noise ratio by a factor of 1.5 compared with fixing $M_i = -4.0$. However, it only increases the distance uncertainty by 0.02 Mpc.

certainty. The SBF signal-to-noise ratio is defined as the SBF signal divided by the uncertainty. We then use the SBF–color relation in [Carlsten et al. \(2019\)](#) to convert the measured SBF signal to distance. The distance uncertainty is derived using Monte Carlo simulations, taking into account the uncertainties in the measured galaxy color, the SBF signal, and the scatter in the SBF–color relation ([Carlsten et al. 2019](#)). We neglect the difference between the Magellan/IMACS and Blanco/DECam *i*-band filters (typically $\lesssim 0.1$ mag difference in the SBF signal, [Carlsten et al. 2022](#)) because it is less dominant than the scatter of color–SBF relation and the measurement uncertainty.

Using the IMACS *i*-band data, the measured SBF distance to Hedgehog is

$$D_{\text{SBF}}^{\text{IMACS}} = 2.41 \pm 0.14 \text{ Mpc},$$

with a signal-to-noise ratio of $\text{SNR} \approx 52$. When using the Legacy Surveys DR10 *i*-band data, the measured SBF distance is

$$D_{\text{SBF}}^{\text{LS}} = 2.45 \pm 0.16 \text{ Mpc},$$

with a signal-to-noise ratio of $\text{SNR} \approx 22$. The distance measurements from two independent datasets perfectly agree with each other. Because the SBF distances from IMACS and Legacy Surveys are very consistent, we take the IMACS distance as the reference value hereafter. This distance corresponds to a distance modulus of $m - M = 26.9 \pm 0.1$ mag.

4. ENVIRONMENT

We explore the environment of Hedgehog by showing its 3-D location with respect to the known galaxies. We take the galaxies in the Updated Nearby Galaxy Catalog (UNGC; [Karachentsev et al. 2013](#)) and calculate their coordinates in the Supergalactic coordinate system. The stellar mass is estimated by taking the K_s -band luminosity in [Karachentsev et al. \(2013\)](#) and assuming a mass-to-light ratio of $M_*/L_{K_s} = 1$ ([Bell et al. 2003](#))⁴. We also calculate the virial radius assuming a stellar-to-halo mass relation from [Rodríguez-Puebla et al. \(2017\)](#) and using *SatGen* ([Jiang et al. 2019](#)).

The left panel of Figure 3 shows the *XY* and *XZ* projections of the 3-D distribution of nearby galaxies. We plot the locations of galaxies relative to Hedgehog for convenience. Hedgehog is shown as a red dot, with the error bar indicating the projected 1σ distance uncertainty. Galaxies that are more massive than

$\log M_*/M_\odot > 9.7$ (1 dex below the stellar mass of MW) are shown as purple circles, with circle size corresponding to the projected virial radius. The fainter blue dots are galaxies with $\log M_*/M_\odot < 9.7$. The dashed circle around Hedgehog indicates a sphere with a radius of 1 Mpc. Hedgehog lives in a low-density environment with no massive neighboring galaxies. The nearest galaxy groups to Hedgehog are the Centaurus A (Cen A) group, the Local Group, and the M83 group. Hedgehog is 1.7 Mpc from Cen A, 2.4 Mpc from MW, and 2.55 Mpc from M83, thus is classified as a field dwarf by the criteria in [Geha et al. \(2012\)](#). The Cen A group has a virial mass ranging from $5.3 \times 10^{12} M_\odot$ ([Müller et al. 2022](#)) to $8 \times 10^{12} M_\odot$ ([Karachentsev et al. 2007](#)), being about 5 – 8 times more massive than the MW ([Patel et al. 2018](#)). Equivalently, Cen A has a virial radius of $R_{\text{vir}} \approx 350 - 410$ kpc. Therefore, Hedgehog is 4 – 5 R_{vir} away from the Cen A group, placing it in a very isolated environment.

We show a close-up view of the 3-D environment in the right panel of Figure 3. Similar to the left panel, the size of the sphere also represents the virial radius of the halo. The Cen A group is shown together with the MW group. We highlight the three closest neighbors of Hedgehog in orange. The closest neighbor of Hedgehog, KKs 53 ([Huchtmeier et al. 2001](#), also known as [KK2000] 53 in [Karachentsev et al. 2013](#) and Cen 7 in [Müller et al. 2017](#)), is 1.00 Mpc away from Hedgehog with a distance of $D_{\text{TRGB}} = 2.93$ Mpc ([Tully et al. 2015](#)) and a K_s -band luminosity of $\log L_{K_s} = 7.46$ ([Karachentsev et al. 2013](#)). The second-closest neighbor is dw1322-39, a dwarf irregular at $D_{\text{TRGB}} = 2.95$ Mpc ([Müller et al. 2019](#)) and $\log L_{K_s} = 6.12$ ([Karachentsev et al. 2013](#)). It is 1.03 Mpc away from Hedgehog and is considered a satellite of the Centaurus A group ([Müller et al. 2019](#)). The third-closest is ESO383-087, located 1.10 Mpc away from Hedgehog. It is a blue dwarf galaxy at $D_{\text{TRGB}} = 3.19$ Mpc with $\log L_{K_s} = 9.05$ ([Karachentsev et al. 2013](#)). Hedgehog’s neighbors are mostly low-mass dwarf galaxies distributed towards the Cen A group. We do not find any neighboring galaxies within 1 Mpc from Hedgehog. This makes Hedgehog one of the most isolated quiescent dwarf galaxies in the Local Volume. As a comparison, Tucana B, whose closest neighbor (IC 5152), is 620 kpc away, is less isolated than Hedgehog. KKs 3 and KKR 25 have a similar degree of isolation as Hedgehog.

5. STRUCTURE AND STELLAR POPULATION

5.1. Luminosity and Size of Hedgehog

We calculate the physical properties of Hedgehog and list them in Table 1. Hedgehog has an effective radius of

⁴ Other authors use a lower mass-to-light ratio than we use here (e.g., [Carlsten et al. 2022](#)), thus the stellar mass and virial radius derived in this work should be considered as upper limits.

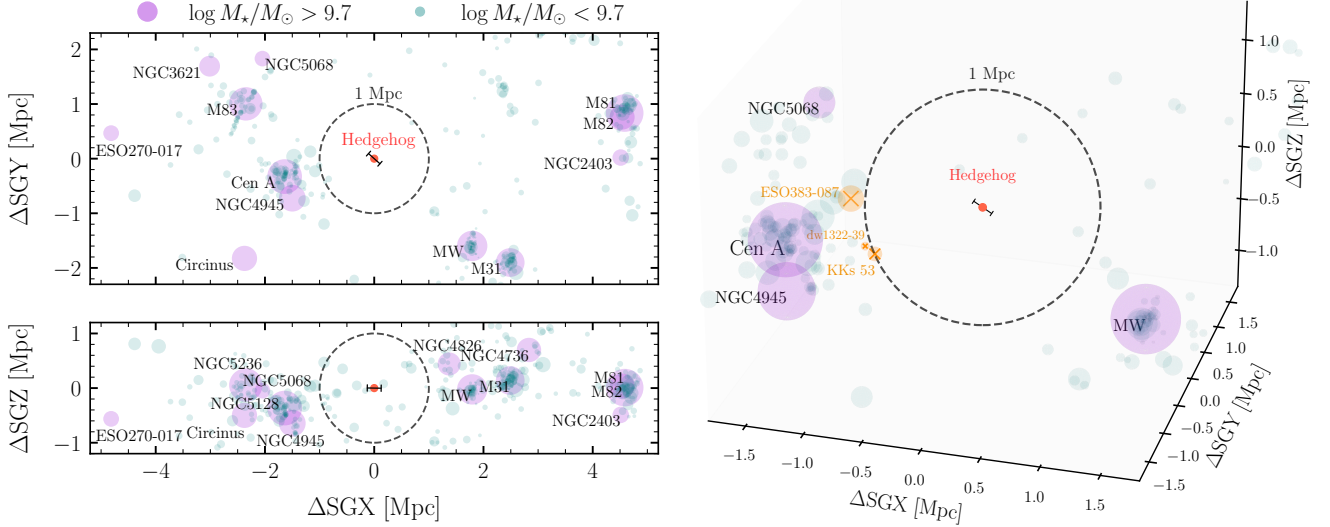


Figure 3. Environment of Hedgehog. We show the distribution of neighboring galaxies from Karachentsev et al. (2013) in the supergalactic coordinates system centered at Hedgehog. The left panel shows the 2-D projected distributions and the right panel provides a close-up view of the environment in 3-D. The size of the circle represents the virial radius of the host halo. Galaxies that are more (less) massive than $M_{\star} = 10^{9.7} M_{\odot}$ are shown in purple (blue). Hedgehog is 1.7 Mpc ($\sim 5.6R_{\text{vir}}$) from its nearest galaxy group Centaurus A. Hedgehog’s closest neighbors, highlighted in orange, are at least 1 Mpc away. Hedgehog is thus one of the most isolated quiescent dwarf galaxies. An interactive version of Figure 3 can be found online <https://astrojacobli.github.io/research/Hedgehog/>.

$r_{\text{eff}} = 176 \pm 14$ pc, and a g -band absolute magnitude of $M_g = -9.56 \pm 0.14$ mag. To compare with the literature, we convert our measured photometry to the V -band using the transformation $V = g - 0.5784 \cdot (g - r) - 0.0038$ ⁵. We also estimate the stellar mass of Hedgehog using the color– M_{\star}/L relation from Into & Portinari (2013), which uses a Kroupa (2001) initial mass function. The derived stellar mass is $M_{\star} = 10^{5.8 \pm 0.1} M_{\odot}$ when using the $g - i$ color, and $M_{\star} = 10^{5.9 \pm 0.1} M_{\odot}$ when using the $g - r$ color. We therefore quote the stellar mass to be $M_{\star} = 10^{5.8 \pm 0.2} M_{\odot}$, considering the uncertainties in photometry, colors, and the color– M_{\star}/L relation.

To place Hedgehog in a broader context, we plot its V -band absolute magnitude and effective radius in Figure 4, together with a few other isolated quiescent dwarf galaxies from the literature. We also show the dwarfs that are considered backplash satellites of MW and M31 as yellow triangles (including Cetus, Tucana, And XVIII, Eri II, Buck et al. 2019; Blaña et al. 2020; Santos-Santos et al. 2023). For reference, we also show the quiescent dwarf galaxies within $D < 2$ Mpc from McConnachie (2012)⁶ and Putman et al. (2021), and also

the early-type satellites of MW analogs at $D < 12$ Mpc from Carlsten et al. (2022). Compared with LG and LV quenched dwarf galaxies, Hedgehog seems to have a smaller size for its luminosity, but is within the scatter of the luminosity–size relation. We also compare the size of Hedgehog with the mass–size relations from Danieli et al. (2018, based on LG dwarfs) and Carlsten et al. (2021, based on LV satellites). Hedgehog sits below both of the average mass–size relations but within the 1.5σ scatter. Therefore, we conclude that Hedgehog is consistent with the mass–size relation of LG and LV dwarfs.

Intriguingly, most isolated quiescent dwarfs (highlighted as diamonds in Figure 4) exhibit smaller sizes compared to the LG and LV quiescent dwarfs. Given that all of these galaxies were discovered serendipitously, it is plausible that their smaller sizes result from observational bias: for a given luminosity, smaller galaxies have higher surface brightnesses and are therefore easier to identify. A homogeneous search for field dwarf galaxies in the Local Volume would provide a more objective assessment of this issue.

5.2. Stellar Population

As described in §2.3, we do not detect significant UV emission from Hedgehog, implying that Hedgehog is a quiescent galaxy. The lack of UV emission indicates the absence of recent star formation on a timescale of

⁵ <https://www.sdss3.org/dr8/algorithms/sdssUBVRITransform.php#Lupton2005>

⁶ <https://www.cadc-ccda.hia-ihh.nrc-cnrc.gc.ca/en/community/nearby/>

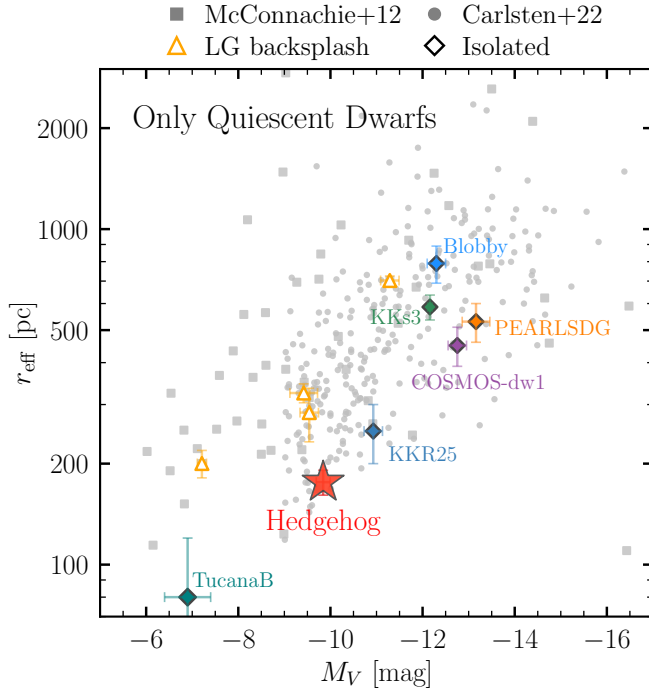


Figure 4. The V -band absolute magnitude and size of Hedgehog, together with other isolated quiescent dwarf galaxies (KKR2, Makarov et al. 2012; KKR33, Karachentsev et al. 2015; Tucana B, Sand et al. 2022; COSMOS-dw1, Polzin et al. 2021; Blobby, Casey et al. 2023; PEARLSDG, Carleton et al. 2024) and potential backplash galaxies in the Local Group (Cetus, Tucana, And XVIII, Eri II; shown in yellow triangle). The quiescent dwarfs at $D < 2$ Mpc (McConnachie 2012) and early-type satellites of MW analogs (Carlsten et al. 2022) are shown in gray for reference. Hedgehog agrees with the luminosity–size relation but is on the smaller side.

< 100 Myr (Lee et al. 2011). To be more precise, we calculate the upper limits of UV-based star formation rates (SFRs) following Equation 3 in Iglesias-Páramo et al. (2006). Similar to Karunakaran et al. (2021), we do not attempt to correct the internal dust extinction because that would require infrared data and also because the dust in dwarf galaxies is likely negligible. The SFR of Hedgehog has an 2σ upper limit of $\text{SFR}_{\text{UV}} \lesssim 10^{-4} M_{\odot} \text{yr}^{-1}$. This limit is similar to or lower than the UV-detected satellites of MW analogs (Karunakaran et al. 2021, 2022). Because the *GALEX* data used here is relatively shallower than the data used in Karunakaran et al. (2022), it is possible that Hedgehog has a much lower SFR than $10^{-4} M_{\odot} \text{yr}^{-1}$.

The integrated color of a dwarf galaxy is often used as a proxy for its stellar population, and the morphology can also roughly represent the stellar population, as early-type dwarfs are typically red and quenched (Carlsten et al. 2021; Greene et al. 2023). Hedgehog has a red

color ($g-r = 0.49$, $g-i = 0.62$) and a symmetric smooth morphology without star-forming regions or dust lanes. Carlsten et al. (2021) derived a luminosity-dependent color cut to separate the early-type satellites from the late-type ones. Given its color, Hedgehog would be classified as early-type according to this relation, consistent with its observed morphology.

To better understand the stellar population, we generate simple stellar populations (SSPs) with various ages and metallicities using the MIST isochrones (Dotter 2016; Choi et al. 2016) and ArtPop (Greco & Danieli 2022), and compare the corresponding colors with the measured colors (Casey et al. 2023). Because of the degeneracy between age and metallicity, we anchor the metallicity of Hedgehog to the metallicity predicted from the mass–metallicity relation from Kirby et al. (2013): $[\text{Fe}/\text{H}] = -1.75 \pm 0.17$. An SSP at this metallicity and with age $t_{\text{age}} = 5-7$ Gyr is consistent with the colors of Hedgehog within the measurement uncertainty. We further validate the inferred stellar population and distance in Appendix B by generating mock galaxy images using ArtPop. However, we cannot rule out the presence of an intermediate-age stellar population ($\sim 0.2-1$ Gyr) with the optical and UV data alone. Deep space-based observation is needed to measure the CMD and derive the star formation history with better temporal resolution (e.g., Makarov et al. 2012; Weisz et al. 2011, 2014).

We also search for neutral gas at the location of Hedgehog and do not find coincident H I detection in the H I Parkes All-Sky Survey (HIPASS; Barnes et al. 2001; Kalberla & Haud 2015) and Galactic All-Sky Survey (GASS; McClure-Griffiths et al. 2009) data. GASS covers a radial velocity range of -400 km s^{-1} to $+500$ km s^{-1} with a higher resolution in velocity, whereas HIPASS covers range of -1280 km s^{-1} to $+12700$ km s^{-1} and is more sensitive than GASS by a factor of 4. However, the radial velocity of Hedgehog is currently unknown. If it is a splashback galaxy from the relatively nearby Cen A group, it might have a similar velocity to Cen A (~ 560 km s^{-1} , Koss et al. 2022). Therefore, the non-detection in GASS might be due to its inadequate velocity range. Using HIPASS, we derive the 3σ upper limit of H I mass to be $M_{\text{HI}} < 10^{6.0} M_{\odot}$, assuming an RMS noise level of 13 mJy and a velocity width of 20 km s^{-1} . The upcoming WALLABY survey (Koribalski et al. 2020), which has a detection limit of $M_{\text{HI}} \sim 10^5 M_{\odot}$ at $D = 2.4$ Mpc, will help us pin down the neutral gas content of Hedgehog.

6. DISCUSSION

Hedgehog is an isolated dwarf galaxy at a distance of 2.41 ± 0.14 Mpc with a stellar mass $M_{\star} \approx 10^{5.8 \pm 0.2} M_{\odot}$.

It has no neighboring galaxies within 1 Mpc, and is 1.7 Mpc ($\sim 4 - 5 R_{\text{vir}}$) from the nearest group, Cen A. Hedgehog is thus one of the most isolated quiescent dwarfs found to date and is less massive than the other extremely isolated dwarfs such as KKs 3 and KKR 25. It shows no sign of recent star formation and has an old stellar population. The challenge is to understand how its star formation is quenched given its isolation.

The most straightforward explanation is that Hedgehog is a backsplash galaxy from the nearest galaxy group. Simulations of satellites around MW-like groups have shown that backsplash galaxies contribute 13% of the dwarf galaxies found between R_{vir} and 1.5 Mpc (Teyssier et al. 2012), and the fraction could be as high as $\sim 50\%$ between R_{vir} and $2.5R_{\text{vir}}$ (Buck et al. 2019). Benavides et al. (2021) even identified a handful of backsplash ultra-diffuse galaxies out to $3 - 4 R_{\text{vir}}$. Similar to satellite galaxies, backsplash galaxies undergo quenching through ram-pressure stripping and tidal interactions, resulting in a quenched fraction comparable to that of the satellites (Simpson et al. 2018).

In the backsplash scenario, Hedgehog is most likely to originate from the Cen A group given their proximity. However, its distance to Cen A might be too far ($\sim 4 - 5 R_{\text{vir}}$) compared with simulations. Given its current distance of 1.7 Mpc from Cen A, Hedgehog’s travel time, assuming an ejection velocity of $v_{\text{esp}} \approx \sqrt{2} v_{\text{circ}}$ with $v_{\text{circ}} \approx 260 \pm 60 \text{ km s}^{-1}$ (Müller et al. 2022), would be 4–6 Gyr. If Hedgehog was quenched within 1–2 Gyr after it had the pericenter passage in the Cen A group (Slater & Bell 2014; Wetzel et al. 2015; Simpson et al. 2018; Greene et al. 2023), the estimated travel time agrees quite well with the inferred age of Hedgehog’s stellar population ($t_{\text{age}} \approx 5 - 7 \text{ Gyr}$).

On the other hand, it might not be surprising at all to find quiescent field dwarfs with $M_{\star} \approx 10^6 M_{\odot}$. Despite that most isolated dwarfs with $M_{\star} = 10^{7-9} M_{\odot}$ are star-forming (Geha et al. 2012), field dwarf galaxies have a quenched fraction of $\sim 20\%$ at $M_{\star} \approx 10^{6-7} M_{\odot}$ (Slater & Bell 2014). Using the empirical galaxy-halo model UNIVERSEMACHINE (Behroozi et al. 2019), Wang et al. (2024) predicted a quenched fraction of $\sim 30\%$ for field dwarfs with $M_{\star} \approx 10^{6.5} M_{\odot}$. In hydrodynamical zoom-in simulations, the quenched fraction ranges from $\sim 25\%$ (Christensen et al. 2024) to $\sim 70\%$ (Simpson et al. 2018) in this mass range.

Several physical mechanisms are invoked to explain quenching in the field. Field dwarfs can have their gas stripped by the ram pressure from the filament gas as they move through the cosmic web (Benítez-Llambay et al. 2013; Simpson et al. 2018). Stellar feedback can contribute to quenching (Samuel et al. 2022), although

it typically results in only temporary quiescence and is unlikely to be the dominant mechanism for field dwarfs. Reionization is most likely to be the dominant quenching mechanism for dwarfs with $M_{\star} \lesssim 10^6 M_{\odot}$ (e.g., Bullock et al. 2001; Ricotti & Gnedin 2005), and isolated quenched dwarfs are the best candidates of reionization fossils (Weisz et al. 2014). The UV background from reionization could blow out the gas via photoevaporation (Rees 1986; Shapiro et al. 2004), prolong gas cooling time by photoionization heating (Efsthathiou 1992), and prevent gas inflow, leading to quenching via starvation (Okamoto et al. 2008; Katz et al. 2020). Hedgehog’s mass is close to the upper limit where reionization can effectively quench star formation. Recent simulations demonstrate that field dwarfs with $M_{\star} \approx 10^{5-6} M_{\odot}$ can be quenched by reionization, but can also be rejuvenated later (Rey et al. 2020). To remain quiescence, it is possible that Hedgehog has a slightly lower halo mass due to the scatter of stellar-to-halo mass relation or experienced a stronger UV background due to the inhomogeneous nature of reionization. The puzzle of Hedgehog’s formation and quenching highlights the complexity of galaxy evolution in the low-mass regime.

Future observations and simulations are needed to fully unveil the formation and evolution of isolated quiescent dwarf galaxies. Polzin et al. (2021) highlight the complexity of stellar populations in many isolated quiescent dwarfs. For Hedgehog, while the integrated colors alone do not rule out the presence of an intermediate-age stellar population, deep CMDs will enable us to uncover its detailed star formation history (e.g., McQuinn et al. 2024). Additionally, Buck et al. (2019) show that backsplash galaxies exhibit lower velocity dispersion compared to field dwarfs. Therefore, radial velocity and velocity dispersion measurements will be crucial in confirming or ruling out the backsplash scenario. With the upcoming Vera C. Rubin Observatory’s Legacy Survey of Space & Time (Ivezić et al. 2019), it will be possible to conduct a blind search for field dwarf galaxies out to $\sim 20 \text{ Mpc}$ with SBF in a homogeneous way, and better characterize quenching as a function of environment and mass.

ACKNOWLEDGMENT

We thank Ava Polzin for curating a list of isolated quiescent dwarf galaxies in the literature⁷. J.L. is grateful for the discussion with Yifei Luo, Shun Wang, Yilun Ma, and Sihao Cheng. J.L. thanks Khalil Fong for his music. J.E.G gratefully acknowledges support from NSF grant

⁷ https://avapolzin.github.io/projects/quench_list/

NSF AAG/AWD1007052. S.D. is supported by NASA through Hubble Fellowship grant HST-HF2-51454.001-A awarded by the Space Telescope Science Institute, which is operated by the Association of Universities for Research in Astronomy, Incorporated, under NASA contract NAS5-26555

This paper includes data gathered with the 6.5 m Magellan Telescopes located at Las Campanas Observatory, Chile.

The DESI Legacy Imaging Surveys consist of three individual and complementary projects: the Dark Energy Camera Legacy Survey (DECaLS), the Beijing-Arizona Sky Survey (BASS), and the Mayall z-band Legacy Survey (MzLS). DECaLS, BASS, and MzLS together include data obtained, respectively, at the Blanco telescope, Cerro Tololo Inter-American Observatory, NSF’s NOIRLab; the Bok telescope, Steward Observatory, University of Arizona; and the Mayall telescope, Kitt Peak National Observatory, NOIRLab. NOIRLab is operated by the Association of Universities for Research in Astronomy (AURA) under a cooperative agreement with the National Science Foundation. Pipeline processing and analyses of the data were supported by NOIRLab and the Lawrence Berkeley National Laboratory (LBNL). Legacy Surveys also uses data products from the Near-Earth Object Wide-field Infrared Survey Explorer (NEOWISE), a project of the Jet Propulsion Laboratory/California Institute of Technology, funded by the National Aeronautics and Space Administration. Legacy Surveys was supported by: the Director, Office of Science, Office of High Energy Physics of the U.S. Department of Energy; the National Energy Research Scientific Computing Center, a DOE Office of Science User Facility; the U.S. National Science Foundation, Division of Astronomical Sciences; the National Astronomical Observatories of China, the Chinese Academy

of Sciences and the Chinese National Natural Science Foundation. LBNL is managed by the Regents of the University of California under contract to the U.S. Department of Energy.

This research used observations made with the NASA Galaxy Evolution Explorer. GALEX is operated for NASA by the California Institute of Technology under NASA contract NAS5-98034.

This research has used the NASA/IPAC Extragalactic Database (NED), which is funded by the National Aeronautics and Space Administration and operated by the California Institute of Technology. This research has also used the NASA/IPAC Infrared Science Archive, which is funded by the National Aeronautics and Space Administration and operated by the California Institute of Technology.

The authors are pleased to acknowledge that the work reported in this paper was substantially performed using the Princeton Research Computing resources at Princeton University, a consortium of groups led by the Princeton Institute for Computational Science and Engineering (PICSciE) and the Office of Information Technology’s Research Computing.

Facilities: Magellan:Baade (IMACS), Blanco (DECam), *GALEX*.

Software: NumPy (Harris et al. 2020), Astropy (Astropy Collaboration et al. 2013, 2018, 2022), SciPy (Jones et al. 2001), Matplotlib (Hunter 2007), ArtPop (Greco et al. 2021), photutils (Bradley et al. 2016), SExtractor (Bertin & Arnouts 1996), SWarp (Bertin et al. 2002), SCAMP (Bertin 2006), astrometry.net (Lang et al. 2010), PSFEx (Bertin 2011), sep (Barbary 2016), imfit (Erwin 2015), sfdmap.

REFERENCES

- Applebaum, E., Brooks, A. M., Christensen, C. R., et al. 2021, ApJ, 906, 96, doi: [10.3847/1538-4357/abcafa](https://doi.org/10.3847/1538-4357/abcafa)
- Astropy Collaboration, Robitaille, T. P., Tollerud, E. J., et al. 2013, A&A, 558, A33, doi: [10.1051/0004-6361/201322068](https://doi.org/10.1051/0004-6361/201322068)
- Astropy Collaboration, Price-Whelan, A. M., Sipőcz, B. M., et al. 2018, AJ, 156, 123, doi: [10.3847/1538-3881/aabc4f](https://doi.org/10.3847/1538-3881/aabc4f)
- Astropy Collaboration, Price-Whelan, A. M., Lim, P. L., et al. 2022, ApJ, 935, 167, doi: [10.3847/1538-4357/ac7c74](https://doi.org/10.3847/1538-4357/ac7c74)
- Barbary, K. 2016, Journal of Open Source Software, 1(6), 58, doi: [10.21105/joss.0005](https://doi.org/10.21105/joss.0005)
- Barnes, D. G., Staveley-Smith, L., de Blok, W. J. G., et al. 2001, MNRAS, 322, 486, doi: [10.1046/j.1365-8711.2001.04102.x](https://doi.org/10.1046/j.1365-8711.2001.04102.x)
- Behroozi, P., Wechsler, R. H., Hearin, A. P., & Conroy, C. 2019, MNRAS, 488, 3143, doi: [10.1093/mnras/stz1182](https://doi.org/10.1093/mnras/stz1182)
- Bell, E. F., McIntosh, D. H., Katz, N., & Weinberg, M. D. 2003, ApJS, 149, 289, doi: [10.1086/378847](https://doi.org/10.1086/378847)
- Benavides, J. A., Sales, L. V., Abadi, M. G., et al. 2021, Nature Astronomy, 5, 1255, doi: [10.1038/s41550-021-01458-1](https://doi.org/10.1038/s41550-021-01458-1)
- Benítez-Llambay, A., Navarro, J. F., Abadi, M. G., et al. 2013, ApJL, 763, L41, doi: [10.1088/2041-8205/763/2/L41](https://doi.org/10.1088/2041-8205/763/2/L41)

- Bertin, E. 2006, in *Astronomical Society of the Pacific Conference Series*, Vol. 351, *Astronomical Data Analysis Software and Systems XV*, ed. C. Gabriel, C. Arviset, D. Ponz, & S. Enrique, 112
- Bertin, E. 2011, in *Astronomical Society of the Pacific Conference Series*, Vol. 442, *Astronomical Data Analysis Software and Systems XX*, ed. I. N. Evans, A. Accomazzi, D. J. Mink, & A. H. Rots, 435
- Bertin, E., & Arnouts, S. 1996, *A&AS*, 117, 393, doi: [10.1051/aas:1996164](https://doi.org/10.1051/aas:1996164)
- Bertin, E., Mellier, Y., Radovich, M., et al. 2002, in *Astronomical Society of the Pacific Conference Series*, Vol. 281, *Astronomical Data Analysis Software and Systems XI*, ed. D. A. Bohlender, D. Durand, & T. H. Handley, 228
- Blaña, M., Burkert, A., Fellhauer, M., Schartmann, M., & Alig, C. 2020, *MNRAS*, 497, 3601, doi: [10.1093/mnras/staa2153](https://doi.org/10.1093/mnras/staa2153)
- Bradley, L., Sipocz, B., Robitaille, T., et al. 2016, *Photutils: Photometry tools*, *Astrophysics Source Code Library*, record ascl:1609.011
- Buck, T., Macciò, A. V., Dutton, A. A., Obreja, A., & Frings, J. 2019, *MNRAS*, 483, 1314, doi: [10.1093/mnras/sty2913](https://doi.org/10.1093/mnras/sty2913)
- Bullock, J. S., Kolatt, T. S., Sigad, Y., et al. 2001, *MNRAS*, 321, 559, doi: [10.1046/j.1365-8711.2001.04068.x](https://doi.org/10.1046/j.1365-8711.2001.04068.x)
- Bullock, J. S., Kravtsov, A. V., & Weinberg, D. H. 2000, *ApJ*, 539, 517, doi: [10.1086/309279](https://doi.org/10.1086/309279)
- Cantiello, M., Blakeslee, J. P., Raimondo, G., et al. 2005, *ApJ*, 634, 239, doi: [10.1086/491694](https://doi.org/10.1086/491694)
- Carleton, T., Ellsworth-Bowers, T., Windhorst, R. A., et al. 2024, *ApJL*, 961, L37, doi: [10.3847/2041-8213/ad1b56](https://doi.org/10.3847/2041-8213/ad1b56)
- Carlsten, S. G., Beaton, R. L., Greco, J. P., & Greene, J. E. 2019, *ApJ*, 879, 13, doi: [10.3847/1538-4357/ab22c1](https://doi.org/10.3847/1538-4357/ab22c1)
- Carlsten, S. G., Greene, J. E., Beaton, R. L., Danieli, S., & Greco, J. P. 2022, *ApJ*, 933, 47, doi: [10.3847/1538-4357/ac6fd7](https://doi.org/10.3847/1538-4357/ac6fd7)
- Carlsten, S. G., Greene, J. E., Greco, J. P., Beaton, R. L., & Kado-Fong, E. 2021, *ApJ*, 922, 267, doi: [10.3847/1538-4357/ac2581](https://doi.org/10.3847/1538-4357/ac2581)
- Casey, K. J., Greco, J. P., Peter, A. H. G., & Davis, A. B. 2023, *MNRAS*, 520, 4715, doi: [10.1093/mnras/stad352](https://doi.org/10.1093/mnras/stad352)
- Choi, J., Dotter, A., Conroy, C., et al. 2016, *ApJ*, 823, 102, doi: [10.3847/0004-637X/823/2/102](https://doi.org/10.3847/0004-637X/823/2/102)
- Christensen, C. R., Brooks, A. M., Munshi, F., et al. 2024, *ApJ*, 961, 236, doi: [10.3847/1538-4357/ad0c5a](https://doi.org/10.3847/1538-4357/ad0c5a)
- Cohen, Y., van Dokkum, P., Danieli, S., et al. 2018, *ApJ*, 868, 96, doi: [10.3847/1538-4357/aae7c8](https://doi.org/10.3847/1538-4357/aae7c8)
- Danieli, S., van Dokkum, P., & Conroy, C. 2018, *ApJ*, 856, 69, doi: [10.3847/1538-4357/aaadfb](https://doi.org/10.3847/1538-4357/aaadfb)
- Dey, A., Schlegel, D. J., Lang, D., et al. 2019, *AJ*, 157, 168, doi: [10.3847/1538-3881/ab089d](https://doi.org/10.3847/1538-3881/ab089d)
- Dotter, A. 2016, *ApJS*, 222, 8, doi: [10.3847/0067-0049/222/1/8](https://doi.org/10.3847/0067-0049/222/1/8)
- Dressler, A., Bigelow, B., Hare, T., et al. 2011, *PASP*, 123, 288, doi: [10.1086/658908](https://doi.org/10.1086/658908)
- Drlica-Wagner, A., Carlin, J. L., Nidever, D. L., et al. 2021, *ApJS*, 256, 2, doi: [10.3847/1538-4365/ac079d](https://doi.org/10.3847/1538-4365/ac079d)
- Drlica-Wagner, A., Ferguson, P. S., Adamów, M., et al. 2022, *ApJS*, 261, 38, doi: [10.3847/1538-4365/ac78eb](https://doi.org/10.3847/1538-4365/ac78eb)
- Efstathiou, G. 1992, *MNRAS*, 256, 43P, doi: [10.1093/mnras/256.1.43P](https://doi.org/10.1093/mnras/256.1.43P)
- El-Badry, K., Quataert, E., Wetzel, A., et al. 2018, *MNRAS*, 473, 1930, doi: [10.1093/mnras/stx2482](https://doi.org/10.1093/mnras/stx2482)
- Erwin, P. 2015, *ApJ*, 799, 226, doi: [10.1088/0004-637X/799/2/226](https://doi.org/10.1088/0004-637X/799/2/226)
- Geha, M., Blanton, M. R., Yan, R., & Tinker, J. L. 2012, *ApJ*, 757, 85, doi: [10.1088/0004-637X/757/1/85](https://doi.org/10.1088/0004-637X/757/1/85)
- Greco, J. P., & Danieli, S. 2022, *ApJ*, 941, 26, doi: [10.3847/1538-4357/ac75b7](https://doi.org/10.3847/1538-4357/ac75b7)
- Greco, J. P., Goulding, A. D., Greene, J. E., et al. 2018, *ApJ*, 866, 112, doi: [10.3847/1538-4357/aae0f4](https://doi.org/10.3847/1538-4357/aae0f4)
- Greco, J. P., van Dokkum, P., Danieli, S., Carlsten, S. G., & Conroy, C. 2021, *ApJ*, 908, 24, doi: [10.3847/1538-4357/abd030](https://doi.org/10.3847/1538-4357/abd030)
- Greene, J. E., Danieli, S., Carlsten, S., et al. 2023, *ApJ*, 949, 94, doi: [10.3847/1538-4357/acc58c](https://doi.org/10.3847/1538-4357/acc58c)
- Gunn, J. E., & Gott, J. Richard, I. 1972, *ApJ*, 176, 1, doi: [10.1086/151605](https://doi.org/10.1086/151605)
- Harris, C. R., Millman, K. J., van der Walt, S. J., et al. 2020, *Nature*, 585, 357, doi: [10.1038/s41586-020-2649-2](https://doi.org/10.1038/s41586-020-2649-2)
- Hopkins, P. F., Quataert, E., & Murray, N. 2012, *MNRAS*, 421, 3522, doi: [10.1111/j.1365-2966.2012.20593.x](https://doi.org/10.1111/j.1365-2966.2012.20593.x)
- Huchtmeier, W. K., Karachentsev, I. D., & Karachentseva, V. E. 2001, *A&A*, 377, 801, doi: [10.1051/0004-6361:20011138](https://doi.org/10.1051/0004-6361:20011138)
- Hunter, J. D. 2007, *Computing in Science Engineering*, 9, 90, doi: [10.1109/MCSE.2007.55](https://doi.org/10.1109/MCSE.2007.55)
- Iglesias-Páramo, J., Buat, V., Takeuchi, T. T., et al. 2006, *ApJS*, 164, 38, doi: [10.1086/502628](https://doi.org/10.1086/502628)
- Into, T., & Portinari, L. 2013, *MNRAS*, 430, 2715, doi: [10.1093/mnras/stt071](https://doi.org/10.1093/mnras/stt071)
- Ivezić, Ž., Kahn, S. M., Tyson, J. A., et al. 2019, *ApJ*, 873, 111, doi: [10.3847/1538-4357/ab042c](https://doi.org/10.3847/1538-4357/ab042c)
- Jiang, F., Dekel, A., Freundlich, J., et al. 2019, *MNRAS*, 487, 5272, doi: [10.1093/mnras/stz1499](https://doi.org/10.1093/mnras/stz1499)
- Jones, E., Oliphant, T., Peterson, P., et al. 2001, *SciPy: Open source scientific tools for Python*. <http://www.scipy.org/>

- Kado-Fong, E., Robinson, A., Nyland, K., et al. 2024, *ApJ*, 963, 37, doi: [10.3847/1538-4357/ad18cb](https://doi.org/10.3847/1538-4357/ad18cb)
- Kalberla, P. M. W., & Haud, U. 2015, *A&A*, 578, A78, doi: [10.1051/0004-6361/201525859](https://doi.org/10.1051/0004-6361/201525859)
- Karachentsev, I. D., Kniazev, A. Y., & Sharina, M. E. 2015, *Astronomische Nachrichten*, 336, 707, doi: [10.1002/asna.201512207](https://doi.org/10.1002/asna.201512207)
- Karachentsev, I. D., Makarov, D. I., & Kaisina, E. I. 2013, *AJ*, 145, 101, doi: [10.1088/0004-6256/145/4/101](https://doi.org/10.1088/0004-6256/145/4/101)
- Karachentsev, I. D., Makarova, L. N., Tully, R. B., Rizzi, L., & Shaya, E. J. 2018, *ApJ*, 858, 62, doi: [10.3847/1538-4357/aabaf1](https://doi.org/10.3847/1538-4357/aabaf1)
- Karachentsev, I. D., Tully, R. B., Dolphin, A., et al. 2007, *AJ*, 133, 504, doi: [10.1086/510125](https://doi.org/10.1086/510125)
- Karunakaran, A., Spekkens, K., Carroll, R., et al. 2022, *MNRAS*, doi: [10.1093/mnras/stac2329](https://doi.org/10.1093/mnras/stac2329)
- Karunakaran, A., Spekkens, K., Oman, K. A., et al. 2021, *ApJL*, 916, L19, doi: [10.3847/2041-8213/ac0e3a](https://doi.org/10.3847/2041-8213/ac0e3a)
- Katz, H., Ramsoy, M., Rosdahl, J., et al. 2020, *MNRAS*, 494, 2200, doi: [10.1093/mnras/staa639](https://doi.org/10.1093/mnras/staa639)
- Kirby, E. N., Cohen, J. G., Guhathakurta, P., et al. 2013, *ApJ*, 779, 102, doi: [10.1088/0004-637X/779/2/102](https://doi.org/10.1088/0004-637X/779/2/102)
- Koribalski, B. S., Staveley-Smith, L., Westmeier, T., et al. 2020, *Ap&SS*, 365, 118, doi: [10.1007/s10509-020-03831-4](https://doi.org/10.1007/s10509-020-03831-4)
- Koss, M. J., Ricci, C., Trakhtenbrot, B., et al. 2022, *ApJS*, 261, 2, doi: [10.3847/1538-4365/ac6c05](https://doi.org/10.3847/1538-4365/ac6c05)
- Kroupa, P. 2001, *MNRAS*, 322, 231, doi: [10.1046/j.1365-8711.2001.04022.x](https://doi.org/10.1046/j.1365-8711.2001.04022.x)
- Lang, D., Hogg, D. W., Mierle, K., Blanton, M., & Roweis, S. 2010, *AJ*, 139, 1782, doi: [10.1088/0004-6256/139/5/1782](https://doi.org/10.1088/0004-6256/139/5/1782)
- Lee, J. C., Gil de Paz, A., Kennicutt, Robert C., J., et al. 2011, *ApJS*, 192, 6, doi: [10.1088/0067-0049/192/1/6](https://doi.org/10.1088/0067-0049/192/1/6)
- Li, J., Greene, J. E., Greco, J. P., et al. 2023, *ApJ*, 955, 1, doi: [10.3847/1538-4357/ace829](https://doi.org/10.3847/1538-4357/ace829)
- Makarov, D., Makarova, L., Sharina, M., et al. 2012, *MNRAS*, 425, 709, doi: [10.1111/j.1365-2966.2012.21581.x](https://doi.org/10.1111/j.1365-2966.2012.21581.x)
- Martin, D. C., Fanson, J., Schiminovich, D., et al. 2005, *ApJL*, 619, L1, doi: [10.1086/426387](https://doi.org/10.1086/426387)
- McClure-Griffiths, N. M., Pisano, D. J., Calabretta, M. R., et al. 2009, *ApJS*, 181, 398, doi: [10.1088/0067-0049/181/2/398](https://doi.org/10.1088/0067-0049/181/2/398)
- McConnachie, A. W. 2012, *AJ*, 144, 4, doi: [10.1088/0004-6256/144/1/4](https://doi.org/10.1088/0004-6256/144/1/4)
- McQuinn, K. B. W., B. Newman, M. J., Savino, A., et al. 2024, *ApJ*, 961, 16, doi: [10.3847/1538-4357/ad1105](https://doi.org/10.3847/1538-4357/ad1105)
- Mei, S., Blakeslee, J. P., Tonry, J. L., et al. 2005, *ApJS*, 156, 113, doi: [10.1086/426544](https://doi.org/10.1086/426544)
- More, S., Diemer, B., & Kravtsov, A. V. 2015, *ApJ*, 810, 36, doi: [10.1088/0004-637X/810/1/36](https://doi.org/10.1088/0004-637X/810/1/36)
- Morrissey, P., Conrow, T., Barlow, T. A., et al. 2007, *ApJS*, 173, 682, doi: [10.1086/520512](https://doi.org/10.1086/520512)
- Müller, O., Jerjen, H., & Binggeli, B. 2017, *A&A*, 597, A7, doi: [10.1051/0004-6361/201628921](https://doi.org/10.1051/0004-6361/201628921)
- Müller, O., Lelli, F., Famaey, B., et al. 2022, *A&A*, 662, A57, doi: [10.1051/0004-6361/202142351](https://doi.org/10.1051/0004-6361/202142351)
- Müller, O., Rejkuba, M., Pawlowski, M. S., et al. 2019, *A&A*, 629, A18, doi: [10.1051/0004-6361/201935807](https://doi.org/10.1051/0004-6361/201935807)
- Okamoto, T., Gao, L., & Theuns, T. 2008, *MNRAS*, 390, 920, doi: [10.1111/j.1365-2966.2008.13830.x](https://doi.org/10.1111/j.1365-2966.2008.13830.x)
- Oke, J. B., & Gunn, J. E. 1983, *ApJ*, 266, 713, doi: [10.1086/160817](https://doi.org/10.1086/160817)
- Patel, E., Besla, G., Mandel, K., & Sohn, S. T. 2018, *ApJ*, 857, 78, doi: [10.3847/1538-4357/aab78f](https://doi.org/10.3847/1538-4357/aab78f)
- Polzin, A., van Dokkum, P., Danieli, S., Greco, J. P., & Romanowsky, A. J. 2021, *ApJL*, 914, L23, doi: [10.3847/2041-8213/ac024f](https://doi.org/10.3847/2041-8213/ac024f)
- Putman, M. E., Zheng, Y., Price-Whelan, A. M., et al. 2021, *ApJ*, 913, 53, doi: [10.3847/1538-4357/abe391](https://doi.org/10.3847/1538-4357/abe391)
- Rees, M. J. 1986, *MNRAS*, 218, 25P, doi: [10.1093/mnras/218.1.25P](https://doi.org/10.1093/mnras/218.1.25P)
- Rey, M. P., Pontzen, A., Agertz, O., et al. 2020, *MNRAS*, 497, 1508, doi: [10.1093/mnras/staa1640](https://doi.org/10.1093/mnras/staa1640)
- Ricotti, M., & Gnedin, N. Y. 2005, *ApJ*, 629, 259, doi: [10.1086/431415](https://doi.org/10.1086/431415)
- Rodríguez-Puebla, A., Primack, J. R., Avila-Reese, V., & Faber, S. M. 2017, *MNRAS*, 470, 651, doi: [10.1093/mnras/stx1172](https://doi.org/10.1093/mnras/stx1172)
- Samuel, J., Wetzell, A., Santistevan, I., et al. 2022, *MNRAS*, 514, 5276, doi: [10.1093/mnras/stac1706](https://doi.org/10.1093/mnras/stac1706)
- Sand, D. J., Mutlu-Pakdil, B., Jones, M. G., et al. 2022, *ApJL*, 935, L17, doi: [10.3847/2041-8213/ac85ee](https://doi.org/10.3847/2041-8213/ac85ee)
- Santos-Santos, I. M. E., Navarro, J. F., & McConnachie, A. 2023, *MNRAS*, 520, 55, doi: [10.1093/mnras/stad085](https://doi.org/10.1093/mnras/stad085)
- Schlafly, E. F., & Finkbeiner, D. P. 2011, *ApJ*, 737, 103, doi: [10.1088/0004-637X/737/2/103](https://doi.org/10.1088/0004-637X/737/2/103)
- Schlegel, D. J., Finkbeiner, D. P., & Davis, M. 1998, *ApJ*, 500, 525, doi: [10.1086/305772](https://doi.org/10.1086/305772)
- Shapiro, P. R., Iliev, I. T., & Raga, A. C. 2004, *MNRAS*, 348, 753, doi: [10.1111/j.1365-2966.2004.07364.x](https://doi.org/10.1111/j.1365-2966.2004.07364.x)
- Simpson, C. M., Grand, R. J. J., Gómez, F. A., et al. 2018, *MNRAS*, 478, 548, doi: [10.1093/mnras/sty774](https://doi.org/10.1093/mnras/sty774)
- Slater, C. T., & Bell, E. F. 2014, *ApJ*, 792, 141, doi: [10.1088/0004-637X/792/2/141](https://doi.org/10.1088/0004-637X/792/2/141)
- Teyssier, M., Johnston, K. V., & Kuhlen, M. 2012, *MNRAS*, 426, 1808, doi: [10.1111/j.1365-2966.2012.21793.x](https://doi.org/10.1111/j.1365-2966.2012.21793.x)
- Tonry, J., & Schneider, D. P. 1988, *AJ*, 96, 807, doi: [10.1086/114847](https://doi.org/10.1086/114847)
- Tully, R. B., Libeskind, N. I., Karachentsev, I. D., et al. 2015, *ApJL*, 802, L25, doi: [10.1088/2041-8205/802/2/L25](https://doi.org/10.1088/2041-8205/802/2/L25)

- Wang, Y., Nadler, E. O., Mao, Y.-Y., et al. 2024, arXiv e-prints, arXiv:2404.14500, doi: [10.48550/arXiv.2404.14500](https://doi.org/10.48550/arXiv.2404.14500)
- Weisz, D. R., Dolphin, A. E., Skillman, E. D., et al. 2014, *ApJ*, 789, 147, doi: [10.1088/0004-637X/789/2/147](https://doi.org/10.1088/0004-637X/789/2/147)
- Weisz, D. R., Dalcanton, J. J., Williams, B. F., et al. 2011, *ApJ*, 739, 5, doi: [10.1088/0004-637X/739/1/5](https://doi.org/10.1088/0004-637X/739/1/5)
- Wetzel, A. R., Tinker, J. L., Conroy, C., & van den Bosch, F. C. 2014, *MNRAS*, 439, 2687, doi: [10.1093/mnras/stu122](https://doi.org/10.1093/mnras/stu122)
- Wetzel, A. R., Tollerud, E. J., & Weisz, D. R. 2015, *ApJL*, 808, L27, doi: [10.1088/2041-8205/808/1/L27](https://doi.org/10.1088/2041-8205/808/1/L27)
- Willmer, C. N. A. 2018, *ApJS*, 236, 47, doi: [10.3847/1538-4365/aabfdf](https://doi.org/10.3847/1538-4365/aabfdf)
- Wyder, T. K., Martin, D. C., Schiminovich, D., et al. 2007, *ApJS*, 173, 293, doi: [10.1086/521402](https://doi.org/10.1086/521402)

APPENDIX

A. MEASUREMENT UNCERTAINTIES AND BIASES

The structural parameters of low surface brightness galaxies are typically obtained by fitting a Sérsic model to the image. However, such measurements are subject to potential biases and uncertainties because of the low-surface-brightness nature of the target galaxies. The measurement could also be biased for those resolved and semi-resolved galaxies. Similar to Li et al. (2023) and Casey et al. (2023), we characterize the measurement biases and uncertainties by generating mock Sérsic galaxy using ArtPop (Greco & Danieli 2022) and compare the measured properties with the ground truth. We use ArtPop models rather than a smooth Sérsic profile to fully mimic the surface brightness fluctuation of Hedgehog and investigate how that would affect the measurement bias and uncertainty.

Assuming the mock galaxies have similar properties (distance, total magnitude, effective radius, Sérsic index, ellipticity) as Hedgehog and have an SSP with an age of 6 Gyr and metallicity of $[\text{Fe}/\text{H}] = -1.75$, we generated 100 different realizations of the mock galaxies with random orientations. These mock galaxies were randomly injected into DECaLS DR10 coadd images within 5 arcmin from Hedgehog (i.e., within the same brick). We ran the Sérsic fitting pipeline for each of these mock galaxies in a similar way to Hedgehog.

The measurement bias is defined as $\Delta X = X_{\text{truth}} - X_{\text{meas}}$, and the measurement uncertainty σ_X is the standard deviation of the measurement difference. The median biases and the uncertainties are listed in Table A. The bias values are typically within the uncertainty range, except for the g -band magnitude m_g and effective radius r_{eff} . The derived biases and uncertainties are comparable to the values in Casey et al. (2023). We then apply bias corrections to the measurement of Hedgehog. The properties of Hedgehog in Table 1 have already been corrected for measurement biases.

B. ARTPOP MODELS

To further demonstrate that the measured distance in §3 and the inferred stellar population in §5 are reasonable, we generate mock Sérsic galaxy images using an SSP with an age of 6 Gyr and metallicity of $[\text{Fe}/\text{H}] = -1.75$ using ArtPop (Greco & Danieli 2022). We place the mock galaxy at 1.8 Mpc, 2.4 Mpc, and 3.0 Mpc, fixing the surface brightness so that the mock galaxy at 2.4 Mpc has the same structural parameters as Hedgehog. The mock galaxy is then injected

Table 2. Measurement Biases and Uncertainties of the Structural Parameters.

Parameter	Uncertainty	Bias
m_g (mag)	± 0.06	0.12
$g - r$ (mag)	± 0.04	-0.02
$g - i$ (mag)	± 0.04	-0.03
r_{eff} (arcsec)	± 0.8	-1.0
$n_{\text{Sérsic}}$	± 0.12	-0.05
Ellipticity	± 0.03	-0.01

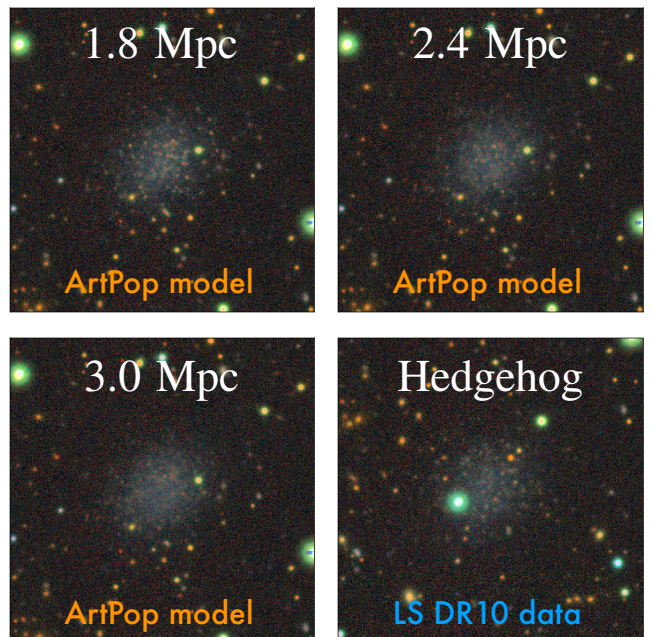


Figure 5. ArtPop models of Hedgehog at different distances. We generate these mock galaxies assuming an SSP with an age of 6 Gyr and metallicity of $[\text{Fe}/\text{H}] = -1.75$ and place them at different distances but fix the shape and surface brightness. The mock galaxy at 2.4 Mpc visually reproduces both the SBF signal and the integrated color of Hedgehog very well. The two galaxies at 1.8 Mpc and 3.0 Mpc show too strong and too weak SBF signals.

into the LS DR10 $griz$ data at $\alpha = 13\text{h}22\text{m}46.99\text{s}$, $\delta = -20\text{d}52\text{m}30.36\text{s}$ (1.5' from Hedgehog), where the data quality is very similar to the location of Hedgehog. The mock images are shown in Figure 5 together with Hedgehog. The mock galaxy at 2.4 Mpc is most similar to Hedgehog in terms of the SBF signal. The integrated color of the mock galaxies also matches the color of Hedgehog quite well.